



ORIGINAL ARTICLE

Characterization, selenylation, and antineoplastic effects on HepG2 cells *in vitro* and *in vivo* of an arabinofuranan from the fruits of *Akebia quinata*



Huimei Wang¹, Zhen Lin¹, Ying Li, Xuelian Wang, Jing Xu*, Yuanqiang Guo*

State Key Laboratory of Medicinal Chemical Biology, College of Pharmacy, and Tianjin Key Laboratory of Molecular Drug Research, Nankai University, Tianjin 300350, People's Republic of China

Received 9 September 2022; accepted 19 November 2022
Available online 25 November 2022

KEYWORDS

Arabinofuranan;
Selenylation;
Akebia quinata;
HepG2 cells;
Zebrafish;
Antiangiogenic

Abstract *Akebia quinata* is a traditional medicinal plant distributed in East Asia and its fruits are applied in food and pharmaceutical fields. Herein, a novel polysaccharide (AQP70-2A) with a molecular weight of 1.49×10^4 Da was isolated from the fruits of *A. quinata*. Results of the chemical and spectroscopic analysis indicated that AQP70-2A was an arabinofuranan with a backbone mainly consisting of $\rightarrow 5$ - α -L-Araf-(1 \rightarrow , $\rightarrow 3,5$)- α -L-Araf-(1 \rightarrow , and $\rightarrow 2,3,5$)- α -L-Araf-(1 \rightarrow , and it also contained two types of branch chains. At the cellular level, AQP70-2A did not show significant antitumor properties, while selenylation significantly made the inhibitory effect of this natural macromolecule on HepG2 cells to be increased. Furthermore, the zebrafish xenograft model confirmed that selenized polysaccharide Se-AQP70-2A effectively blocked hepatocellular carcinoma cells invasion and metastasis. Meanwhile, the inhibition of Se-AQP70-2A on development of intersegmental vessels revealed its antiangiogenic activity.

© 2022 The Author(s). Published by Elsevier B.V. on behalf of King Saud University. This is an open access article under the CC BY license (<http://creativecommons.org/licenses/by/4.0/>).

1. Introduction

According to the latest statistics, there were 19.29 million new cancer cases and 9.96 million cancer deaths worldwide in 2020, of which liver cancer cases and deaths accounted for 4.7 % and 8.3 %, respectively (Sung et al., 2021). Although liver cancer ranks sixth in terms of global incidence, it is the second leading cause of cancer deaths in men. Globally, over 80 % of primary liver cancers are caused by hepatocellular carcinoma (HCC) (El-Serag and Rudolph, 2007) and has a 5-year survival rate of only 30–40 % (Zhong et al., 2017). Tumor metastasis is an important cause of death in HCC patients (Chen et al., 2008). Reduced the tumor metastasis can be achieved by inhibiting the migration, invasion, and adhesion of metastatic cells. However, there is little advancement in the field of tumor metastasis blocking (Huang et al., 2015). In order to better prevent and treat HCC or other tumors, there is an

* Corresponding authors.

E-mail addresses: xujing611@nankai.edu.cn (J. Xu), victgyq@nankai.edu.cn (Y. Guo).

¹ These authors contributed equally to this work.

Peer review under responsibility of King Saud University.



Production and hosting by Elsevier

urgent need for novel molecules with anti-cancer and anti-metastasis activities. Recently, the severe side effects of chemotherapeutic drugs have prompted interest in natural low-toxicity active molecules, and increasing potential natural molecules for the treatment of HCC have been reported from traditional Chinese herbs and dietary plants (Lu et al., 2018; Hsu et al., 2011; Tsai et al., 2013). In addition to small molecules, natural biological macromolecular polysaccharides have been proved to be effective in the treatment of HCC, which can inhibit tumor growth by targeting vascular endothelial growth factor, improving cytokine expression level and regulating immunity (Wang et al., 2017b).

Selenium is an essential trace element, and plays a critical role in reparation of cellular damage and immunoenhancement (Wang et al., 2018; Wei et al., 2015). Moreover, increasing evidences have shown that selenium exerts immunomodulatory effects on HCC by regulating oxidative stress, inflammation, angiogenesis, and apoptosis, implying that selenium supplementation has a potential preventive and therapeutic function on HCC (Darvesh and Bishayee, 2010; Wu et al., 2021). Compared with inorganic selenium, organic selenium has the advantages of high absorption rate and low toxicity, and is a suitable way of selenium supplement for long-term use (Wang et al., 2018). Among organic selenium, the study of selenium polysaccharides is a hot topic in recent years. However, due to the low content of this type of organic selenium in natural resources, selenylation modification has become an effective way to prepare selenized polysaccharides (Wang et al., 2018; Lee et al., 2017). The bioactivity of selenium polysaccharides is not simply the superposition of selenium and polysaccharide activities, but may achieve a distinctive pharmacological profile (Wen et al., 2019), which expands the potential application of natural polysaccharides in medicine and functional foods.

Akebia quinata (Houtt.) Decne. is a creeping woody vine, which belongs to the Lardizabalaceae family and is widely distributed over East Asia (Choi et al., 2005). The fruits of *A. quinata*, known as “Bayuezha” in Chinese, have been commonly used in traditional Chinese medicines as an analgesic, an antiphlogistic, and a diuretic (Sung et al., 2015). Moreover, the fruits of *A. quinata* can be consumed as a dietary supplement, such as processed fruit vinegar and juice (Wang et al., 2015; Du et al., 2012). Previous reports indicated that polysaccharides were the important active ingredients in the water extract of *A. quinata*, and these macromolecules were found to have potential anticancer and immunomodulatory activities (Wang et al., 2022; Wang, et al., 2021). However, research on polysaccharides in this traditional medicine is still preliminary. Even in the same species, the natural polysaccharides are a series of molecules with different structures (Seedeve et al., 2018).

The great structural diversity of natural polysaccharides confers these molecules a variety of activity, which are therefore considered as a new source of drug development (Adami et al., 2018). In order to further refine the comprehensive description of polysaccharides in fruits of *A. quinata*, this work aims to explore the chemical information of novel macromolecules with structures different from those of polysaccharides previously reported. Meanwhile, the potential anti-hepatocarcinoma activity of their selenized products was evaluated.

2. Materials and methods

2.1. Materials and chemicals

The detailed information of materials and reagents used in presented study can be found in the Supplementary information.

2.2. Isolation and purification of polysaccharide

The crude polysaccharide was prepared by extracting the fruits of *A. quinata* according to our previous report (Wang, et al., 2021). Firstly, the dried medicinal herbs (5.0 kg) were extracted with hot water (90 °C) three times at 1:6 g/mL for two hours each time. As the solid residue was filtered out, the filtrate was con-

centrated under reduced pressure to one tenth of its original volume, and then centrifuged to collect the supernatant. Anhydrous ethanol was added into the concentrated extract to adjust the final concentration to 50 % and 70 %, respectively. Then, the 70 % precipitation was deproteinized with Sevag reagent (dichloromethane: *n*-butanol = 4: 1, v/v) (Hoseiniyan Benvidi and Jahanbin, 2020), followed by dialysis (3500 Da cut-off) and freeze drying to obtain crude polysaccharide named AQ70.

AQ70 was applied to DEAE-Sepharose Fast Flow (DEAE-FF) column (Ø 3.5 × 40 cm) and eluted first with distilled water, and then with gradient concentration NaCl solution (0.05, 0.1, and 0.2 M) at 1.0 mL/min flow rate. The fraction eluted with 0.05 M NaCl was collected and named AQ70-2. Furthermore, AQ70-2 was purified by Sephadex G-75 gel filtration column (Ø 1.5 × 100 cm) at 0.8 mL/min flow rate. The first elution band was collected and AQP70-2A was harvested successively by concentration and freeze-drying.

2.3. Purity, homogeneity and molecular weight analysis

The UV-visible spectrophotometer was employed to perform band scanning at 200–400 nm to detect the presence of nucleic acids and proteins in the polysaccharides sample. Furthermore, the molecular parameters of AQP70-2A were determined by high performance size exclusion chromatography (HPSEC) in line with previous report (Wang et al., 2022). Detailed information about the operation process can be found in the Supplementary information.

2.4. Identification of monosaccharide composition

The monosaccharide composition of AQP70-2A was analyzed according to the method previously reported (Zhang et al., 2020a). The Supplementary information shows the detailed description of the experiment procedures.

2.5. Fourier transform infrared spectrum and methylation analysis

The dried AQP70-2A sample (1 mg) was ground with potassium bromide powder before pressed into sheets, and analyzed by Fourier transform infrared (FT-IR) spectrometer under a wave number range of 4000 to 400 cm⁻¹.

Glycosidic linkages of the polysaccharide were determined by methylation analysis as described previously (Zhang et al., 2020). The detailed steps of methylation analysis are given in the Supplementary information.

2.6. NMR analysis

The ¹H NMR, ¹³C NMR, DEPT-135 NMR, HSQC, and HMBC were recorded using a 400 MHz Bruker AV-400 spectrometer (Bremen, Germany), and analyzed by MestReNova software (Version 11.0.1, Mestrelab Research SL, Spain).

2.7. Congo red assay

The solution of polysaccharide was mixed with Congo red reagent, and NaOH was added to adjust the final concentration

to 0, 0.1, 0.2, 0.3, 0.4, 0.5, and 0.6 M, respectively. The maximum absorption wavelength (λ_{\max}) of Congo red-polysaccharide complexes at various concentrations of NaOH was observed.

2.8. Scanning electron microscope (SEM) analysis

The dried AQP70-2A sample (1 mg) was coated with a conductive layer of gold–palladium and applied to FE-SEM (JOEL, JSM-7800F, Tokyo, Japan) at an accelerating voltage of 15.0 kV.

2.9. Preparation of selenium-modified polysaccharide

The dried polysaccharide (20 mg) was dissolved in 5 mL HNO_3 (0.6 %, v/v) and stirred at room temperature for 30 min. Then Na_2SeO_3 and BaCl_2 were added to the mixture, and the reaction lasted for 8 h with stirring under 65 °C. The pH value of the reaction mixture was adjusted to 7–8 with NaOH, and the Ba^{2+} was removed with sodium sulfate. After dialysis, the reaction product was precipitated with ethanol, and the selenium-modified polysaccharide named Se-AQP70-2A was recovered by freeze-drying. Chemical characterization of Se-AQP70-2A was performed using the methods consistent with natural polysaccharides. Meanwhile, SEM equipped with energy dispersive spectrometer (EDS) was used to semi-quantitatively measure Se element content of Se-AQP70-2A. Accurate quantification of Se element was performed by applying the samples to the inductively couple plasma mass spectrometry (ICP-MS) platform.

2.10. Effects of polysaccharides on HepG2 cells viability

Human hepatocellular carcinoma cell line HepG2 was selected as a model and MTT assay was used to evaluate the antitumor activity of polysaccharides *in vitro*. The detailed procedure of cell viability assessment is summarized in the [Supplementary information](#).

2.11. Evaluation of antitumor activity *in vivo*

Zebrafish, a vertebrate model, has been widely used in pharmacological and toxicological studies due to its high homology with human and its transparent body at the early developmental stages, which is easy to observe the changes of tissue structure ([Gu et al., 2021](#); [Gu et al., 2022](#)). According to the reported methods ([Liang et al., 2020](#)), the *in vivo* activity of polysaccharides against tumor cell invasion and metastasis was evaluated in a zebrafish tumor xenograft model. Meanwhile, the anti-angiogenic activity of Se-AQP70-2A was evaluated using the transgenic zebrafish *Tg (fli1: EGFP)* and compared with the positive control treated with 1 $\mu\text{g}/\text{mL}$ sunitinib malate ([Wang et al., 2021](#)). The detailed procedure of *in vivo* experimental are presented in the [Supplementary information](#).

2.12. Statistical analysis

The experimental data were statistically analyzed using GraphPad Prism 7.0 software and presented as mean \pm standard deviation. Significant differences between different groups were analyzed by one-way ANOVA followed by Turkey's multiple range tests.

3. Results and discussion

3.1. Isolation and purification of AQP70-2A

The percentage yield of crude polysaccharide (AQ70) separated by alcohol precipitation was 1.3 % (polysaccharides weight/ dried fruits weight). The elution profiles of AQ70 was shown in Fig S1A. There were two elution bands within the elution range of 0.05 M NaCl, and the first peak was collected with the yield of 0.2 % (polysaccharides weight/ dried fruits weight) and named AQP70-2. Anion-exchange chromatographic elution products were further purified, and AQP70-2 was divided into two components named AQP70-2A and AQP70-2B by Sephadex G-75 column ([Fig. S1B](#)). The percentage yield of the two fractions AQP70-2A and AQP70-2B purified by molecular sieve both amounted to 0.02 % (polysaccharides weight/ dried fruits weight).

3.2. Homogeneity and molecular weight of AQP70-2A

The UV–vis spectrum showed that there were no characteristic absorption peaks at 260 nm and 280 nm ([Fig. S2B](#)), indicating no proteins and nucleic acids present in AQP70-2A. Moreover, AQP70-2A was eluted as a single peak in HPGPC ([Fig. S2A](#)), suggesting it was a homogenous polysaccharide with a narrow molecular weight distribution. In addition, the sugar content test showed that the carbohydrate content in AQP70-2A was 95.41 %. The calibration curve was obtained by plotting the retention time of the serial Dextran standards versus the logarithm of the molecular weight ([Fig. S3](#); [Table S1](#)). The average molecular weight of AQP70-2A was calculated to be 1.49×10^4 Da according to the standard calibration curve. Furthermore, HPSEC-MALLS-RI system was used to determine the molecular parameters of polysaccharide ([Fig. S4](#); [Table 1](#)). The number-average molecular weight (M_n), weight-average molecular weight (M_w) and z-average molecular weight (M_z) of AQP70-2A were calculated to be 1.49×10^4 , 1.53×10^4 , and 1.56×10^4 g/mol, respectively. The M_w/M_n and M_z/M_n as polydispersity indexes for evaluating the molecular weight distribution width of AQP70-2A were 1.023 and 1.047, respectively, which suggested the molecular weight distribution of AQP70-2A was narrow. The data were consistent with the results of HPGPC analysis, confirming that AQP70-2A was a homogeneous polysaccharide.

3.3. Monosaccharide composition of AQP70-2A

Compared with the retention time of the standard monosaccharide, the PMP pre-derivatization method showed that the AQP70-2A was composed only of arabinose ([Fig. S5](#)). AQP70-2A was a homopolysaccharide different from AQP70-2B, which was also eluted by 0.05 M NaCl, and AQP70-2B was a heteropolysaccharide composed of rhamnose, glucose, galactose and arabinose ([Wang et al., 2022](#)).

3.4. Glycosidic linkages analysis of AQP70-2A

The disappearance of the O–H band ($3100\text{--}3700\text{ cm}^{-1}$) in the IR spectrum of the methylated AQP70-2A indicated that hydroxyl (–OH) was replaced with methoxy groups (–OCH₃),

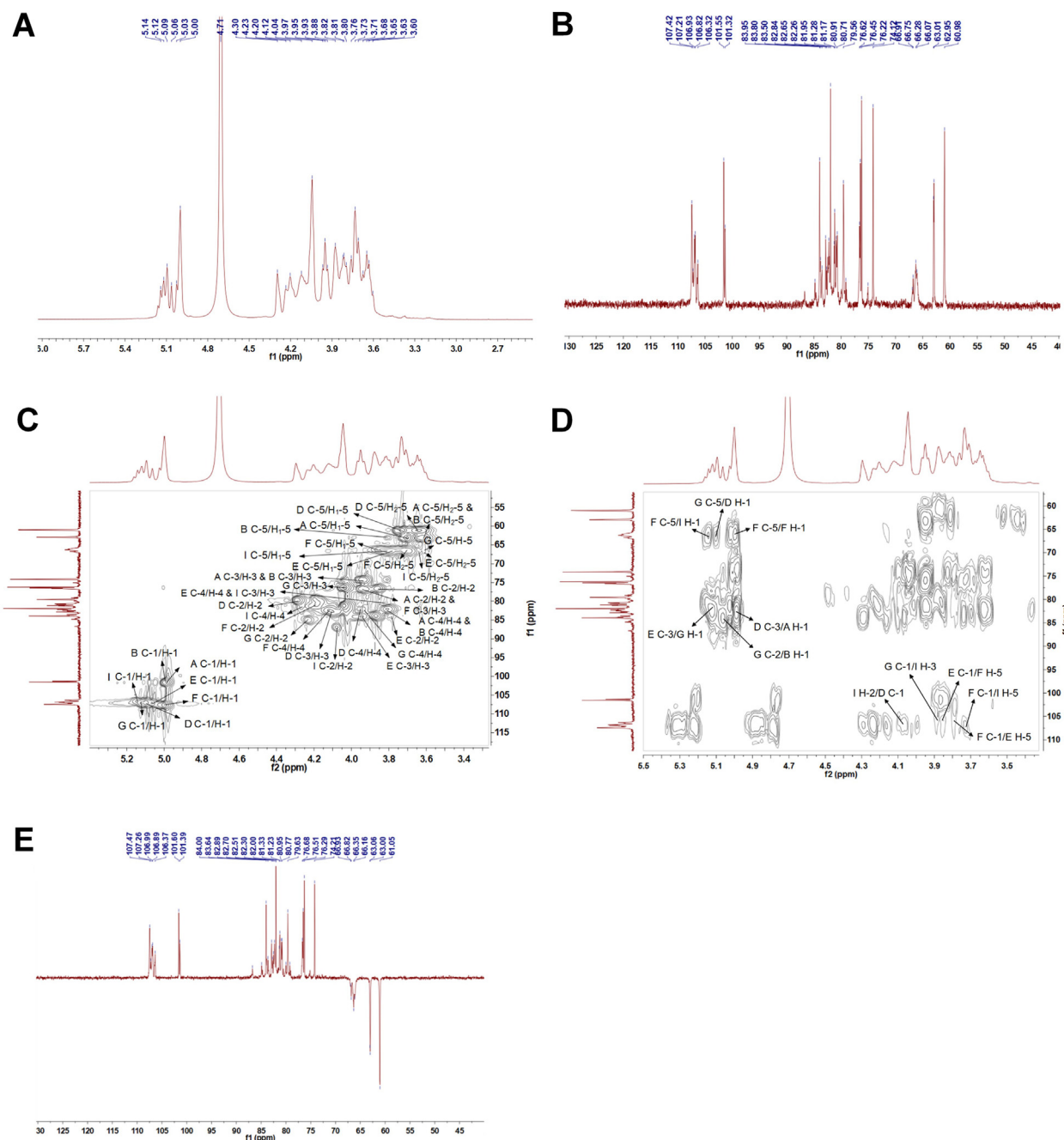


Fig. 1 NMR analysis of AQP70-2A. (A) The ^1H NMR spectrum of AQP70-2A. (B) The ^{13}C NMR spectrum of AQP70-2A. (C) The HSQC spectrum of AQP70-2A. (D) The HMBC spectrum of AQP70-2A. (E) The DEPT-135 NMR spectrum of AQP70-2A.

which confirmed that the methylation reaction of the polysaccharides was complete (Fig. S6). By analyzing mass spectrometry of PMAAs (Fig. S7), the linkage patterns of monosaccharide residues were shown in Table S2. Methylation analysis showed that the AQP70-2A was composed of 1-substituted, 1,3-disubstituted, 1,5-disubstituted, 1,2,5-trisubstituted, 1,3,5-trisubstituted, and 1,2,3,5-tetrasubstituted-L-arabinose residues. The detection of tetra-substituted monosaccharide residues suggested that AQP70-2A was a novel arabinan different from that previously reported (Wang et al., 2021).

3.5. NMR spectroscopy analysis of AQP70-2A

The primary structure of AQP70-2A was further derived comprehensively by NMR spectra. From the ^1H NMR spectrum (Fig. 2A), six anomeric proton signals were shown clearly at 5.00, 5.03, 5.06, 5.09, 5.12, and 5.14 ppm. The ratio of the integral areas of these anomeric proton signals was appropriately calculated as 5.80: 1.40: 1.27: 2.44: 1.91: 1, respectively. In the spectral region 3.60–4.30 ppm, the signals were non-anomeric protons of sugar ring (H-2 – H-5). In the anomeric carbon region (90–110 ppm), the ^{13}C NMR spectrum of AQP70-2A

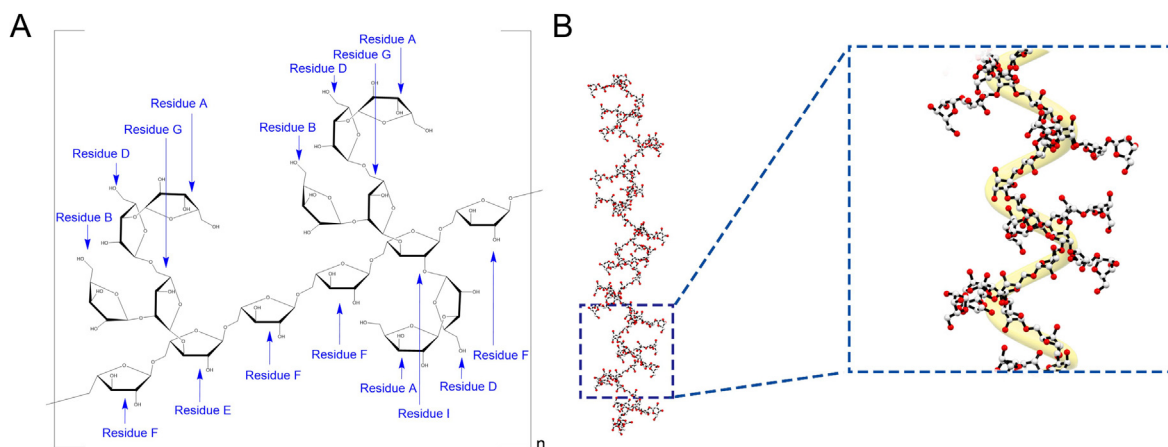


Fig. 2 (A) The putative structure of AQP70-2A. (B) The possible stretching state of AQP70-2A in 0.1 M NaCl solution.

Table 1 The molecular weight parameters of AQP70-2A.

Molecular characteristics	Parameter	Detection results
Polydispersity (PDI)	M_w/M_n	1.023
	M_z/M_n	1.047
Molar mass moments (g/mol)	M_w	1.53×10^4
	M_n	1.49×10^4
	M_z	1.56×10^4

exhibited seven anomeric carbon signals (Fig. 2B). Among these resonance peaks of anomeric carbon, the signals at 107.4, 107.2, 106.9, 106.8, and 106.3 ppm could be assigned to five different α -L-arabinose residues, while signals at 101.6 and 101.3 ppm were attributed to β -L-arabinose residues (Cardoso et al., 2002; Dourado et al., 2006). According to the literature, methylene carbon atom (C-5) of arabinose contributed to the six inverted carbon signals (61.0, 63.0, 66.1, 66.3, 66.8, and 66.9 ppm) in DEPT-135 spectrum (Fig. 2E) (Das et al., 2013).

The ^1H and ^{13}C chemical shift assignments of AQP70-2A shown in Table 2 were determined according to the spectral information in the 1D and 2D NMR experiments and by comparison with the NMR data from arabinans or arabinan rich-polysaccharides (Zhang et al., 2020a; Zhang et al., 2020b; Cardoso et al., 2002; Dourado et al., 2006; Shakhmatov et al., 2014; Fernandes et al., 2019; Rodrigues et al., 2019; Shakhmatov et al., 2015). Based on the literature (Cardoso et al., 2002; Dourado et al., 2006), the H-1/C-1 cross peaks at 5.00/101.6 and 5.03/101.3 ppm in HSQC spectrum (Fig. 2C) indicated that the polysaccharides contained two types of t- β -L-Araf in different chemical environments, named residues A and B, respectively. Combining with the ^1H , ^{13}C , and HSQC spectra, the strongest signal at 5.00/107.4 ppm was assigned to $\rightarrow 5$ - α -L-Araf-(1 \rightarrow) (residue F) due to its high molar ratio in methylation analysis. Meanwhile, the correlation in ^1H - ^1H COSY spectrum (Fig. S8) allowed the assignments of non-anomeric chemical shifts of residue F (H-2 at δ 5.00, H-3 at δ 4.18, H-4 at δ 3.95, H-5/5' at δ 3.84/3.72), and these chemical shift characteristics were found to be close to

those observed in the literature (Zhang et al., 2020a; Shakhmatov et al., 2014). Moreover, in the HSQC spectrum, the correlations at 5.09/106.8, 5.06/107.2, 5.12/106.9 and 5.14/106.3 ppm were also be attributed to α -L-Araf (Zhang et al., 2020b; Fernandes et al., 2019), and these residues were designated as D, E, G and I, respectively. The other carbon and proton signals in the residues were assigned according to ^1H - ^1H COSY and HSQC spectra. The downfield shift of C-3 confirmed the presence of the 3-*O* substituted (82.8 ppm), which indicated that the residue D was $\rightarrow 3$ - α -L-Araf-(1 \rightarrow) (Rodrigues et al., 2019). Compared with 1,5-disubstituted-L-arabinose residue, the HSQC spectrum showed a downfield shift for C-3 (83.9 ppm) in residue E, and a downfield shift for C-2 (84.8 ppm) in residue G, suggesting that the residues E and G were 1,3,5-trisubstituted and 1,2,5-trisubstituted α -L-arabinofuranose, respectively. Similarly, the significant glycosylation shifts of C-2, C-3 and C-5 in residue I indicated that the unit was 1,2,3,5-tetrasubstituted-L-arabinose residue (Shakhmatov et al., 2015).

The HMBC spectrum was applied to further confirm the sequence of arabinose residues in AQP70-2A (Fig. 2D). In detail, the cross peak of δ_{H} 5.00 (residue F, H-1) and δ_{C} 66.3 (residue F, C-5) in the HMBC spectrum, indicated that the AQP70-2A contained two residues F connected through 1,5 linkages. Moreover, HMBC correlations of $\delta_{\text{H/C}}$ 3.84/107.2 (F H-5/E C-1), 3.79/107.4 (E H-5/F C-1), 5.14/66.3 (I H-1/F C-5), 5.09/66.9 (D H-1/G C-5), and 3.76/107.4 (I H-5/F C-1) supported that the *O*-5 of residue F was linked to C-1 of residue E, the *O*-5 of residue E was linked to C-1 of residue F, the *O*-1 of residue I was linked to C-5 of residue F, the *O*-1 of residue D was linked to C-5 of residue G, and the *O*-5 of residue I was linked to C-1 of residue F. Similarly, the bonding information of polysaccharide branch chain residues can be characterized as follows: C-3 signal of $\rightarrow 3,5$ - α -L-Araf-(1 \rightarrow) correlated with H-1 signal of $\rightarrow 2,5$ - α -L-Araf-(1 \rightarrow), C-2 signal of $\rightarrow 2,5$ - α -L-Araf-(1 \rightarrow) correlated with H-1 signal of β -L-Araf-(1 \rightarrow) (residue B), C-5 signal of $\rightarrow 2,5$ - α -L-Araf-(1 \rightarrow) correlated with H-1 signal of $\rightarrow 3$ - α -L-Araf-(1 \rightarrow), C-2 signal of $\rightarrow 2,3,5$ - α -L-Araf-(1 \rightarrow) correlated with H-1 signal of $\rightarrow 3$ - α -L-Araf-(1 \rightarrow), and H-3 signal of $\rightarrow 2,3,5$ - α -L-Araf-(1 \rightarrow) correlated with C-1 signal of $\rightarrow 2,5$ - α -L-Araf-(1 \rightarrow). Further, residue A linked to the end of the branched chain could be verified by the cross peaks of δ_{H} 5.00 (A H-1) and δ_{C} 82.8 (D C-3). The above sig-

Table 2 ^1H and ^{13}C NMR chemical shift assignments (δ in ppm) of AQP70-2A based the HSQC and HMBC spectra.

Residue	H-1	H-2	H-3	H-4	H-5
	C-1	C-2	C-3	C-4	C-5
β -L-Araf-(1 \rightarrow)	5.00	3.95	3.95	3.82	3.73/3.63
Residue A	101.6	76.7	74.1	81.9	63.0
β -L-Araf-(1 \rightarrow)	5.03	3.88	3.95	3.82	3.82/3.65
Residue B	101.3	76.4	74.1	81.9	63.0
\rightarrow 3)- α -L-Araf-(1 \rightarrow)	5.09	4.30	4.10	3.97	3.73/3.63
Residue D	106.8	79.6	82.8	82.3	61.0
\rightarrow 3,5)- α -L-Araf-(1 \rightarrow)	5.06	3.80	3.95	3.85	3.79/3.63
Residue E	107.2	83.5	83.9	80.9	66.1
\rightarrow 5)- α -L-Araf-(1 \rightarrow)	5.00	4.18	3.95	4.13	3.84/3.72
Residue F	107.4	81.2	76.6	82.5	66.3
\rightarrow 2,5)- α -L-Araf-(1 \rightarrow)	5.12	4.24	4.05	3.93	3.62/3.59
Residue G	106.9	84.8	76.2	80.7	66.9
\rightarrow 2,3,5)- α -L-Araf-(1 \rightarrow)	5.14	4.08	3.85	4.27	3.76/3.65
Residue I	106.3	86.7	80.9	81.3	66.8

nal attribution matched with the characteristic signals of several arabinose residues reported in the literature (Makarova and Shakhmatov 2020; Zhang et al., 2019). Based on all the structural evidence, AQP70-2A was an arabinan composed of seven kinds of sugar residues, and its putative structure of AQP70-2A was displayed in Fig. 2.

3.6. Congo red test of AQP70-2A

Compared with those of Congo red, the maximum absorption wavelengths of AQP70-2A plus Congo red did not change significantly with the change of NaOH concentration, which indicated that AQP70-2A was absent of triple-helix structure (Fig. S9).

3.7. Conformation analysis

The slope of the fitting curve in the conformation plot of AQP70-2A was calculated to be 0.38 (Fig. S4C), indicating that the branching polymer presented a compact coil chain conformation (Wang et al., 2022). The possible stretching state of the AQP70-2A simulated by employed Chem 3D was shown in Fig. 2B, which was consistent with the conformation analysis.

3.8. FT-IR analysis of polysaccharides

The FT-IR infrared spectrum of AQP70-2A was shown in Fig. S10A. Specifically, the absorption bands at 3400 cm^{-1} and 2932 cm^{-1} correspond to stretching vibration of O—H and C—H, respectively (Xiang et al., 2019). The absorption bands at 1647 cm^{-1} can be attributed to the O—H bending vibration. Moreover, the bands in the region of 1419 cm^{-1} , 1363 cm^{-1} , and 1220 cm^{-1} were assigned to C—H bending vibration (Hu et al., 2019; Li et al., 2021). According to the literature (Zheng et al., 2020), the typical absorption bands between 1200 and 1000 cm^{-1} were dominated by the sugar ring vibrations and the overlapped stretching vibrations of C—OH side groups and the C—O—C glycosidic bonds. As reported in the literature, the absorption band at 807 cm^{-1} was caused by furanose rings, suggesting that the AQP70-2A contained furan sugar residues (Jahanbin et al., 2017).

Se-AQP70-2A and AQP70-2A shared the same main characteristic bands, meaning that the basic skeleton remained unchanged (Fig. S10B). Se-AQP70-2A showed two absorption bands at 860 cm^{-1} and 805 cm^{-1} , corresponding to the stretching vibrations of Se = O and C—O—Se. In accordance with the previous experimental findings, these absorption bands confirmed that selenylation occurred in AQP70-2A (Wang et al., 2022; Zhu et al., 2016; Wei et al., 2015).

3.9. SEM-EDS analysis of polysaccharides

Surface morphology of AQP70-2A was observed with SEM (Fig. S11). As shown in the $957\times$ image, AQP70-2A had rod-like morphological features. Further SEM image at higher magnifications ($2000\times$) clearly showed that the surface of AQP70-2A presented a porous structure with a hollow interior similar to that of a honeycomb.

SEM images of Se-AQP70-2A provided surface morphological information (Fig. 3A). In contrast to the morphology of native polysaccharide (Fig. S11), Se-AQP70-2A exhibited a relatively continuous surface with local undulation and folds, which was much smoother than that before selenylation modification. These changes suggested that the presence of selenium significantly changed the rough and irregular surface characteristics of the polymer, as reported by Ru et al. (2020).

Energy dispersive spectrometer (EDS) images indicated a homogeneous distribution of C, O, and Se elements in AQP70-2A (Fig. 3B, D—F), and the contents of these three elements were calculated to be 59.8 %, 39.9 %, and 0.3 % (Fig. 3C), respectively. While, the ICP-MS test was performed to reveal that accurate content of Se element in Se-AQP70-2A was 0.92 %. The content data were consistent with those reported in the literature, which were between 0.11 and 0.91 % in selenylation polysaccharide samples prepared by the method $\text{Na}_2\text{SeO}_3\text{-HNO}_3$ (Cheng et al., 2018).

3.10. Inhibitory effect of AQP70-2A and Se-AQP70-2A on HepG2 cell viability

MTT assay results indicated that in the tested concentration range ($25\text{--}400\text{ }\mu\text{g/mL}$), the natural polysaccharide AQP70-2A had weak effects on the viability of cancer cells *in vitro*

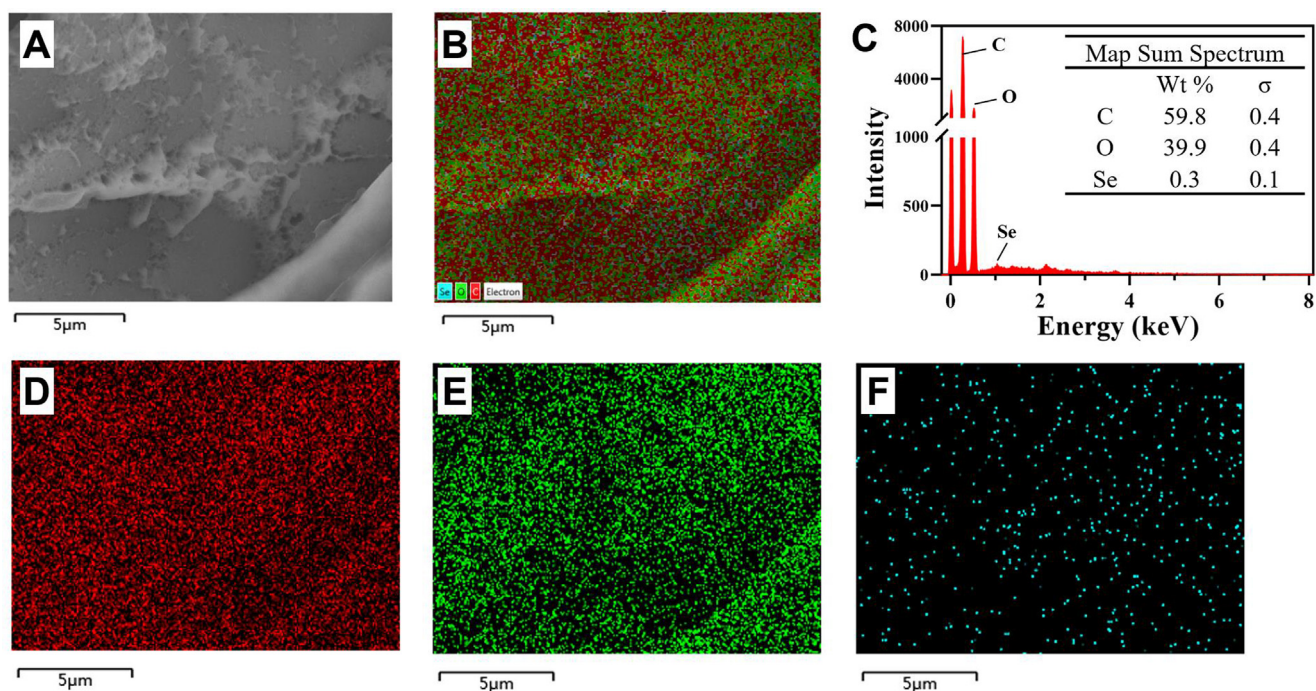


Fig. 3 SEM-EDS analysis of Se-AQP70-2A. (A and B) SEM images and element distribution of Se-AQP70-2A. (C) Surface elemental composition of Se-AQP70-2A. (D–F) Carbon, oxygen, and selenium element distribution of Se-AQP70-2A.

(Fig. S12). After selenylation, the inhibitory activity of polysaccharides on cancer cells was enhanced in a dose-dependent manner, especially in the concentration range of 100–400 $\mu\text{g}/\text{mL}$, the inhibition rate was significantly up-regulated, which was 7 to 10 times than that of AQP70-2A. The half maximal inhibitory concentration (IC_{50}) of Se-AQP70-2A on HepG2 viability was calculated to be 191.4 $\mu\text{g}/\text{mL}$.

3.11. anti-metastasis and anti-angiogenesis effect of Se-AQP70-2A *in vivo*

Red fluorescent-labeled cancer cells and disseminated foci from tumor mass in the xenograft model were observed under confocal microscopy (Fig. 4). With Se-AQP70-2A administration, the total fluorescence intensity and the number of disseminated foci *in vivo* model decreased significantly in a dose dependent manner. These two indices were down-regulated by 44.4 % and 30.7 % in 200 $\mu\text{g}/\text{mL}$ Se-AQP70-2A-treated group, respectively, which was almost consistent with the anti-tumor invasion and metastasis effects of lentinan (LNT) (200 $\mu\text{g}/\text{mL}$) used as a positive control. These results implied that Se-AQP70-2A played an anticancer role by effectively blocking tumor invasion and metastasis.

Furthermore, the antiangiogenic effects of Se-AQP70-2A were evaluated by the development of intersegmental vessels (ISVs) in transgenic zebrafish model *Tg(fli1:EGFP)* (Fig. 5). Se-AQP70-2A treatment significantly inhibited the growth of ISVs, in which the ISVs total lengths of zebrafish in the 25, 50, and 100 $\mu\text{g}/\text{mL}$ concentration groups were approximately 9.26 %, 31.5 %, and 33.3 % shorter than those of the control group, respectively. The antiangiogenic activity of 100 $\mu\text{g}/\text{mL}$

Se-AQP70-2A could reach 85.6 % of sunitinib malate as the positive control.

4. Discussion

The chemical composition and structural characteristics of polysaccharides determine their potential biological activities (Li et al., 2019). Natural polysaccharides have been reported to inhibit tumor cell growth (Wang et al., 2022; Zhan et al., 2021). In contrast, AQP70-2A has no significant effect on the proliferation of HepG2 *in vitro*, and the differences in activity could be attributed to the distinct in primary structure including molecular weight and monosaccharide composition.

After the introduction of selenium into the sugar chain, AQP70-2A exhibited superior anti-tumor function. Compared with Se-AQP70-2B contained similar selenium content, Se-AQP70-2A showed a higher tumor cell inhibition rate. Selenium content was presumed to be the key factor affecting the antitumor activity of selenium containing polymer *in vitro* (Wang et al., 2017). Moreover, it has been reported the bioactivities of selenized polysaccharides were also affected by carbohydrate content (Qin et al., 2013). Therefore, the difference in antitumor activity between Se-AQP70-2A and Se-AQP70-2B indicated that the anticancer activity of selenium-modified polysaccharide was not only related to selenium content, but also depended on the chemical characteristics of the carbohydrate.

The contributing factors for selenylation modification to enhance the inhibitory effects of AQP70-2A on cancer cells could be divided into two aspects. Firstly, selenium-containing polysaccharides act as organic selenium supplements to mediate cancer cell toxicity (He et al., 2013). The

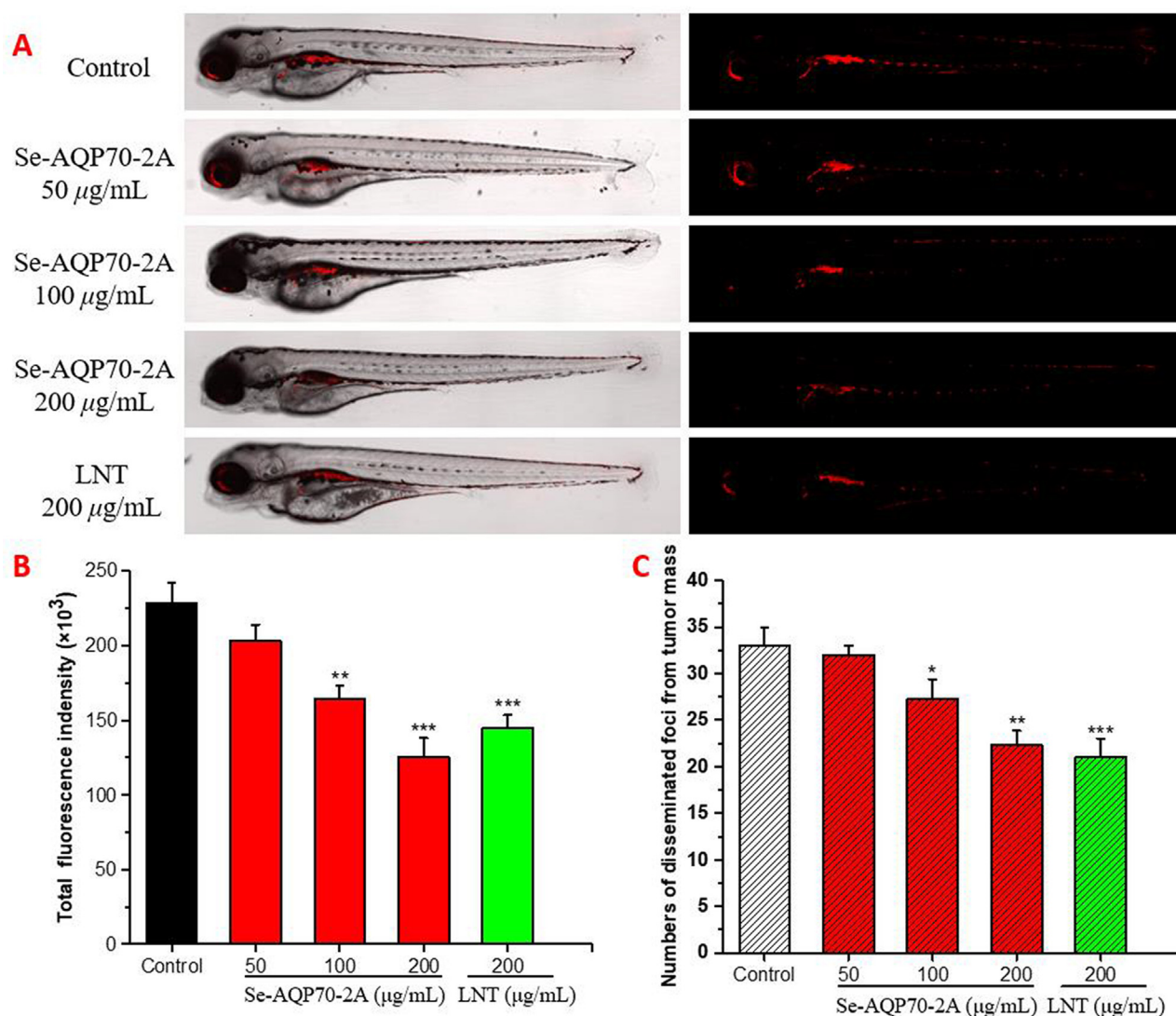


Fig. 4 Antineoplastic effects of Se-AQP70-2A cells in zebrafish xenograft. After transplanting CM-Dil stained HepG2 cells into 2 dpf zebrafish embryos via microinjection, tumor-bearing embryos were treated with Se-AQP70-2A (50, 100, and 200 $\mu\text{g/mL}$). (A) Intensity and distribution of the red fluorescence were observed under a confocal microscope. (B) Fluorescence intensity of the tumor xenografts, representing the number of HepG2 cells. (C) Quantification of the fluorescent area of the tumor xenografts, representing HepG2 cells metastasis. The data expressed as mean \pm SD ($n = 15/\text{group}$). * $p < 0.05$, ** $p < 0.01$, and *** $p < 0.001$ versus control group.

combination of selenium and polysaccharide improved the application limitation of inorganic selenium with low bioavailability and high toxicity (Zhou et al., 2022).

Besides, the bioactivity of selenium polysaccharides is not a simple superposition of selenium and polysaccharide activities, but may achieve a distinctive pharmacological profile while enhancing the bioactivity (Wen et al., 2019). The introduction of Se may change the advanced structure of AQP70-2A, which could be observed from the SEM surface structure analysis. The bioactive properties of selenized polysaccharides were strongly associated with spatial conformation (Li et al., 2019). Selenylation may change the high-level structure of carbohydrate chain, making AQP70-2A acquire distinctive pharmacological functions.

The anti-proliferation mechanism of selenized polysaccharides included arresting the S phase of cancer cells, upregulating the intracellular ROS level, and activating caspase-3 to

induce apoptosis (Li et al., 2017). Moreover, both selenium and polysaccharide can individually exert anti-metastasis and anti-angiogenesis effects by regulating the expression of matrix metalloproteinase (MMPs) and tissue inhibitor of metalloproteinase (TIMPs) (Varghese et al., 2017; Chen et al., 2013). The biological mechanism of Se-AQP70-2 inhibiting tumor development still needs further investigation.

5. Conclusion

This study investigated the structural properties of a natural polysaccharide AQP70-2A isolated from *A. quinata*. Meanwhile, the potential anti-hepatocarcinoma activity of selenized polysaccharide product Se-AQP70-2A was investigated. Analysis performed with AQP70-2A revealed that it was an arabinan with an average molecular weight of 1.49×10^4 Da. The main skeleton of AQP70-2A was composed of three sugar residues $\rightarrow 5)\text{-}\alpha\text{-L-Araf-(1}\rightarrow, \rightarrow 3,5)\text{-}\alpha\text{-L-Araf-(1}\rightarrow,$

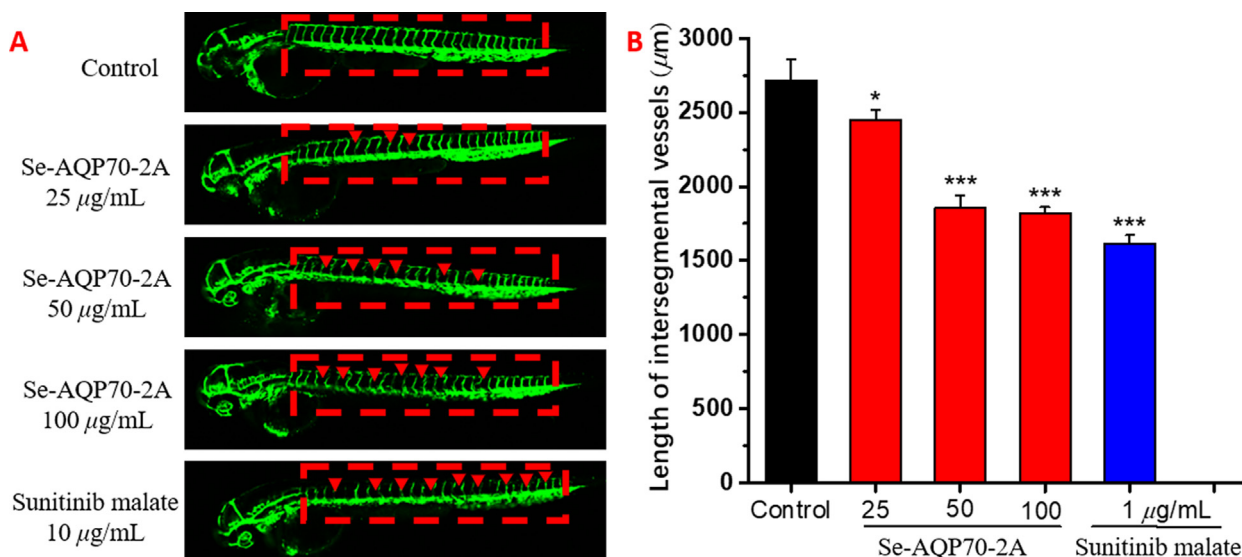


Fig. 5 Antiangiogenic activity of Se-AQP70-2A. The anti-angiogenic activity of Se-AQP70-2A (25, 50, and 100 µg/mL) was evaluated using the transgenic zebrafish *Tg (fli1: EGFP)* and compared with positive control treated with 1 µg/mL sunitinib malate. (A) The development of intersegmental vessels (ISVs) and dorsal longitudinal anastomotic vessels (DLAVs) in different groups. (B) The average length of ISVs of zebrafish after treating with different concentrations of Se-AQP70-2A. The data expressed as mean ± SD (n = 15/group). **p* < 0.05, ****p* < 0.001 versus control group.

and → 2,3,5)- α -L-Araf-(1 →. Each repeating unit contained two types of branch chain. This natural polysaccharide AQP70-2A was not observed significant inhibition of HepG2 cells viability *in vitro*. The selenized polysaccharide Se-AQP70-2A prepared by Na₂SeO₃-HNO₃ method significantly improved the inhibitory effects on HepG2 cells. Compared with positive control LNT, Se-AQP70-2A also exhibited anti-hepatocarcinoma activity by effectively blocking the invasion and metastasis of HepG2 cells *in vivo*. Furthermore, the anti-angiogenic property of Se-AQP70-2A was confirmed by the transgenic zebrafish model. This work explored a novel arabinofuranan from the fruits of *A. quinata*, which further investigate the chemical composition of this plant from the standpoint of biological macromolecules. Meanwhile, the potential anti-hepatocarcinoma activity of Se-AQP70-2A implied its application in pharmaceutical and functional food fields.

Declaration of Competing Interest

The authors declare that they have no known competing financial interests or personal relationships that could have appeared to influence the work reported in this paper.

Acknowledgments

This research was supported financially by the National Natural Science Foundation of China (Nos. 22277059, 22177054, and 22077067), and the National Key Research and Development Program of China (No. 2018YFA0507204).

Appendix A. Supplementary material

Supplementary data to this article can be found online at <https://doi.org/10.1016/j.arabjc.2022.104448>.

References

Adami, E.R., Corso, C.R., Turin-Oliveira, N.M., Galindo, C.M., Milani, L., Stipp, M.C., do Nascimento, G.E., Chequin, A., da

- Silva, L.M., de Andrade, S.F., Dittrich, R.L., Queiroz-Telles, J.E., Klassen, G., Ramos, E.A.S., Cordeiro, L.M.C., Acco, A., 2018. Antineoplastic effect of pectic polysaccharides from green sweet pepper (*Capsicum annuum*) on mammary tumor cells *in vivo* and *in vitro*. *Carbohydr. Polym.* 201, 280–292. <https://doi.org/10.1016/j.carbpol.2018.08.071>.
- Cardoso, S.M., Silva, A.M., Coimbra, M.A., 2002. Structural characterization of the olive pomace pectic polysaccharide arabinan side chains. *Carbohydr. Res.* 337 (10), 917–924. [https://doi.org/10.1016/S0008-6215\(02\)00082-4](https://doi.org/10.1016/S0008-6215(02)00082-4).
- Chen, Y.C., Prabhu, K.S., Mastro, A.M., 2013. Is selenium a potential treatment for cancer metastasis? *Nutrients* 5 (4), 1149–1168. <https://doi.org/10.3390/nu5041149>.
- Chen, N., Sun, W., Deng, X., Hao, Y., Chen, X., Xing, B., Jia, W., Ma, J., Wei, H., Zhu, Y., Qian, X., Jiang, Y., He, F., 2008. Quantitative proteome analysis of HCC cell lines with different metastatic potentials by SILAC. *Proteomics* 8 (23–24), 5108–5118. <https://doi.org/10.1002/pmic.200800280>.
- Cheng, L., Wang, Y., He, X., Wei, X., 2018. Preparation, structural characterization and bioactivities of Se-containing polysaccharide: A review. *Int. J. Biol. Macromol.* 120 (Pt A), 82–92. <https://doi.org/10.1016/j.ijbiomac.2018.07.106>.
- Choi, J., Jung, H.J., Lee, K.T., Park, H.J., 2005. Antinociceptive and anti-inflammatory effects of the saponin and sapogenins obtained from the stem of *Akebia quinata*. *J. Med. Food* 8 (1), 78–85.
- Darvesh, A.S., Bishayee, A., 2010. Selenium in the prevention and treatment of hepatocellular carcinoma. *Anti-Cancer Agent Me* 10 (4), 338–345. <https://doi.org/10.2174/187152010791162252>.
- Das, D., Maiti, S., Maiti, T.K., Islam, S.S., 2013. A new arabinoxylan from green leaves of *Litsea glutinosa* (Lauraceae): structural and biological studies. *Carbohydr. Polym.* 92 (2), 1243–1248. <https://doi.org/10.1016/j.carbpol.2012.10.052>.
- Dourado, F., Cardoso, S., Silva, A., Gama, F., Coimbra, M., 2006. NMR structural elucidation of the arabinan from *prunus dulcis* immunobiological active pectic polysaccharides. *Carbohydr. Polym.* 66 (1), 27–33. <https://doi.org/10.1016/j.carbpol.2006.02.020>.
- Du, Y., Jiang, Y., Zhu, X., Xiong, H., Shi, S., Hu, J., Peng, H., Zhou, Q., Sun, W., 2012. Physicochemical and functional properties of the protein isolate and major fractions prepared from *akebia trifoliata*

- var. *australis* seed. Food Chem. 133, 923–929. <https://doi.org/10.1016/j.foodchem.2012.02.005>.
- El-Serag, H.B., Rudolph, K.L., 2007. Hepatocellular carcinoma: epidemiology and molecular carcinogenesis. Gastroenterology 132 (7), 2557–2576. <https://doi.org/10.1053/j.gastro.2007.04.061>.
- Fernandes, P., Silva, A., Evtuguin, D.V., Nunes, F.M., Wessel, D.F., Cardoso, S.M., Coimbra, M.A., 2019. The hydrophobic polysaccharides of apple pomace. Carbohydr. Polym. 223, <https://doi.org/10.1016/j.carbpol.2019.115132> 115132.
- Gu, J., Guo, M., Zheng, L., Yin, X., Zhou, L., Fan, D., Shi, L., Huang, C., Ji, G., et al., 2021. Protective effects of lignin-carbohydrate complexes from wheat stalk against bisphenol A neurotoxicity in zebrafish via oxidative stress. Antioxidants 10 (10), 1640.
- Gu, J., Guo, M., Yin, X., Huang, C., Qian, L., Zhou, L., Wang, Z., Wang, L., Shi, L., Ji, G., 2022. A systematic comparison of neurotoxicity of bisphenol A and its derivatives in zebrafish. Sci. Total Environ. 805, 150210.
- He, N., Shi, X., Zhao, Y., Tian, L., Wang, D., Yang, X., 2013. Inhibitory effects and molecular mechanisms of selenium-containing tea polysaccharides on human breast cancer MCF-7 cells. J. Agr. Food Chem. 61 (3), 579–588. <https://doi.org/10.1021/jf3036929>.
- Hoseiniyan Benvidi, S.M., Jahanbin, K., 2020. A new water-soluble polysaccharide from *Echinops pungens* Trautv roots. Part I. Isolation, purification, characterization and antioxidant activity. Int. J. Biol. Macromol. 161, 909–916. <https://doi.org/10.1016/j.ijbiomac.2020.06.128>.
- Hsu, C.-L., Shyu, M.-H., Lin, J.-A., Yen, G.-C., Fang, S.-C., 2011. Cytotoxic effects of geranyl flavonoid derivatives from the fruit of *Artocarpus communis* in SK-Hep-1 human hepatocellular carcinoma cells. Food Chem. 127 (1), 127–134. <https://doi.org/10.1016/j.foodchem.2010.12.100>.
- Hu, Z., Zhou, H., Li, Y., Wu, M., Yu, M., Sun, X., 2019. Optimized purification process of polysaccharides from *Carex meyeriana* Kunth by macroporous resin, its characterization and immunomodulatory activity. Int. J. Biol. Macromol. 132, 76–86. <https://doi.org/10.1016/j.ijbiomac.2019.03.207>.
- Huang, F.K., Han, S., Xing, B., Huang, J., Liu, B., Bordeleau, F., Reinhart-King, C.A., Zhang, J.J., Huang, X.Y., 2015. Targeted inhibition of fascin function blocks tumour invasion and metastatic colonization. Nat. Commun. 6, 7465. <https://doi.org/10.1038/ncomms8465>.
- Jahanbin, K., Abbasian, A., Ahang, M., 2017. Isolation, purification and structural characterization of a new water-soluble polysaccharide from *Eremurus stenophyllus* (boiss. & buhse) baker roots. Carbohydr. Polym. 178, 386–393. <https://doi.org/10.1016/j.carbpol.2017.09.058>.
- Lee, J.H., Lee, Y.K., Chang, Y.H., 2017. Effects of selenylation modification on structural and antioxidant properties of pectic polysaccharides extracted from *Ulmus pumila* L. Int. J. Biol. Macromol. 104 (Pt A), 1124–1132. <https://doi.org/10.1016/j.ijbiomac.2017.06.121>.
- Li, Z., An, L., Zhang, S., Shi, Z., Bao, J., Tuerhong, M., Abudukeremu, M., Xu, J., Guo, Y., 2021. Structural elucidation and immunomodulatory evaluation of a polysaccharide from *Stevia rebaudiana* leaves. Food Chem. 364, <https://doi.org/10.1016/j.foodchem.2021.130310> 130310.
- Li, J., Shen, B., Nie, S., Duan, Z., Chen, K., 2019. A combination of selenium and polysaccharides: Promising therapeutic potential. Carbohydr. Polym. 206, 163–173. <https://doi.org/10.1016/j.carbpol.2018.10.088>.
- Li, H., Wang, Y., Wang, C., Zhang, S., Li, S., Zhou, G., Wang, S., Zhang, J., 2017. Extraction, selenylation modification and antitumor activity of the glucan from *Castanea mollissima* Blume. Glycoconj. J. 34 (2), 207–217. <https://doi.org/10.1007/s10719-016-9753-4>.
- Liang, Y., Zhang, Q., Yang, X., Li, Y., Zhang, X., Li, Y., Du, Q., Jin, D.Q., Cui, J., Lall, N., Tuerhong, M., Lee, D., Abudukeremu, M., Xu, J., Shuai, L., Guo, Y., 2020. Diterpenoids from the leaves of *Casearia kurzii* showing cytotoxic activities. Bioorg. Chem. 98, <https://doi.org/10.1016/j.bioorg.2020.103741> 103741.
- Lu, C., Li, C., Chen, B., Shen, Y., 2018. Composition and antioxidant, antibacterial, and anti-HepG2 cell activities of polyphenols from seed coat of *Amygdalus pedunculata* Pall. Food Chem. 265, 111–119. <https://doi.org/10.1016/j.foodchem.2018.05.091>.
- Makarova, E.N., Shakhmatov, E.G., 2020. Structural characteristics of oxalate-soluble polysaccharides from Norway spruce (*Picea abies*) foliage. Carbohydr. Polym. 246, <https://doi.org/10.1016/j.carbpol.2020.116544> 116544.
- Qin, T., Chen, J., Wang, D., Hu, Y., Wang, M., Zhang, J., Nguyen, T. L., Liu, C., Liu, X., 2013. Optimization of selenylation conditions for Chinese angelica polysaccharide based on immune-enhancing activity. Carbohydr. Polym. 92 (1), 645–650. <https://doi.org/10.1016/j.carbpol.2012.08.097>.
- Rodrigues, J.M., Duarte, M., Noseda, M.D., 2019. Modified soybean meal polysaccharide with high adhesion capacity to *Salmonella*. Int. J. Biol. Macromol. 139, 1074–1084. <https://doi.org/10.1016/j.ijbiomac.2019.08.038>.
- Ru, Y., Liu, K., Kong, X., Li, X., Shi, X., Chen, H., 2020. Synthesis of selenylated polysaccharides from *Momordica charantia* L. and its hypoglycemic activity in streptozotocin-induced diabetic mice. Int. J. Biol. Macromol. 152, 295–304. <https://doi.org/10.1016/j.ijbiomac.2020.02.288>.
- Seedei, P., Moovendhan, M., Sudharsan, S., Sivasankar, P., Sivakumar, L., Vairamani, S., Shanmugam, A., 2018. Isolation and chemical characteristics of rhamnose enriched polysaccharide from *Grateloupia lithophila*. Carbohydr. Polym. 195, 486–494. <https://doi.org/10.1016/j.carbpol.2018.05.002>.
- Shakhmatov, E.G., Toukach, P.V., Michailowa, C., Makarova, E.N., 2014. Structural studies of arabinan-rich pectic polysaccharides from *Abies sibirica* L. Biological activity of pectins of *A. sibirica*. Carbohydr. Polym. 113, 515–524. <https://doi.org/10.1016/j.carbpol.2014.07.037>.
- Shakhmatov, E.G., Udoratina, E.V., Atukmaev, K.V., Makarova, E. N., 2015. Extraction and structural characteristics of pectic polysaccharides from *Abies sibirica* L. Carbohydr. Polym. 123, 228–236. <https://doi.org/10.1016/j.carbpol.2015.01.041>.
- Sung, H., Ferlay, J., Siegel, R.L., Laversanne, M., Soerjomataram, I., Jemal, A., Bray, F., 2021. Global Cancer Statistics 2020: GLOBOCAN Estimates of Incidence and Mortality Worldwide for 36 Cancers in 185 Countries. CA Cancer J. Clin. 71 (3), 209–249. <https://doi.org/10.3322/caac.21660>.
- Sung, Y.Y., Kim, D.S., Kim, H.K., 2015. *Akebia quinata* extract exerts anti-obesity and hypolipidemic effects in high-fat diet-fed mice and 3T3-L1 adipocytes. J. Ethnopharmacol. 168, 17–24. <https://doi.org/10.1016/j.jep.2015.03.051>.
- Tsai, K.H., Hsien, H.H., Chen, L.M., Ting, W.J., Yang, Y.S., Kuo, C. H., Tsai, C.H., Tsai, F.J., Tsai, H.J., Huang, C.Y., 2013. Rhubarb inhibits hepatocellular carcinoma cell metastasis via GSK-3 β activation to enhance protein degradation and attenuate nuclear translocation of β -catenin. Food Chem. 138 (1), 278–285. <https://doi.org/10.1016/j.foodchem.2012.10.038>.
- Varghese, S., Joseph, M.M., S, R., Sreelekha, T.T., 2017. T.3he inhibitory effect of anti-tumor polysaccharide from *Punica granatum* on metastasis. Int. J. Biol. Macromol. 103, 1000–1010. <https://doi.org/10.1016/j.ijbiomac.2017.05.137>.
- Wang, X., Ding, J., Feng, Y., Weng, L., Zhao, G., Xiang, J., Zhang, M., Xing, D., 2017b. Targeting of growth factors in the treatment of hepatocellular carcinoma: The potentials of polysaccharides. Oncol. Lett. 13 (3), 1509–1517. <https://doi.org/10.3892/ol.2017.5602>.
- Wang, L., Li, X., Wang, B., 2018. Synthesis, characterization and antioxidant activity of selenium modified polysaccharides from

- Hohenbuehelia serotina*. Int. J. Biol. Macromol. 120 (Pt B), 1362–1368. <https://doi.org/10.1016/j.ijbiomac.2018.09.139>.
- Wang, H., Li, Y., Wang, X., Li, Y., Cui, J., Jin, D.Q., Tuerhong, M., Abudukeremu, M., Xu, J., Guo, Y., 2022. Preparation and structural properties of selenium modified heteropolysaccharide from the fruits of *Akebia quinata* and *in vitro* and *in vivo* antitumor activity. Carbohydr. Polym. 278,. <https://doi.org/10.1016/j.carbpol.2021.118950> 118950.
- Wang, D.P., Liu, K.L., Li, X.Y., Lu, G.Q., Xue, W.H., Qian, X.H., Mohamed, O.K., Meng, F.H., 2021a. Design, synthesis, and *in vitro* and *in vivo* anti-angiogenesis study of a novel vascular endothelial growth factor receptor-2 (VEGFR-2) inhibitor based on 1,2,3-triazole scaffold. Eur. J. Med. Chem. 211,. <https://doi.org/10.1016/j.ejmech.2020.113083> 113083.
- Wang, J., Ren, H., Xu, Q.L., Zhou, Z.Y., Wu, P., Wei, X.Y., Cao, Y., Chen, X.X., Tan, J.W., 2015. Antibacterial oleanane-type triterpenoids from pericarps of *Akebia trifoliata*. Food Chem. 168, 623–629. <https://doi.org/10.1016/j.foodchem.2014.07.105>.
- Wang, H., Wang, X., Li, Y., Zhang, S., Li, Z., Li, Y., Cui, J., Lan, X., Zhang, E., Yuan, L., Jin, D.Q., Tuerhong, M., Abudukeremu, M., Xu, J., Guo, Y., 2021b. Structural properties and *in vitro* and *in vivo* immunomodulatory activity of an arabinofuranan from the fruits of *Akebia quinata*. Carbohydr. Polym. 256,. <https://doi.org/10.1016/j.carbpol.2020.1117521>.
- Wang, J., Yang, X., Bao, A., Liu, X., Zeng, J., Liu, X., Yao, J., Zhang, J., Lei, Z., 2017a. Microwave-assisted synthesis, structure and anti-tumor activity of selenized *Artemisia sphaerocephala* polysaccharide. Int. J. Biol. Macromol. 95, 1108–1118.
- Wei, D., Chen, T., Yan, M., Zhao, W., Li, F., Cheng, W., Yuan, L., 2015. Synthesis, characterization, antioxidant activity and neuro-protective effects of selenium polysaccharide from *Radix hedysari*. Carbohydr. Polym. 125, 161–168. <https://doi.org/10.1016/j.carbpol.2015.02.029>.
- Wen, Z.S., Tang, Z., Gu, L.X., Xiang, X.W., Qu, Y.L., 2019. Immunomodulatory effect of low molecular-weight seleno-aminopolysaccharide on immunosuppressive mice. Int. J. Biol. Macromol. 123, 1278–1288. <https://doi.org/10.1016/j.ijbiomac.2018.10.099>.
- Wu, B.K., Chen, Q.H., Pan, D., Chang, B., Sang, L.X., 2021. A novel therapeutic strategy for hepatocellular carcinoma: Immunomodulatory mechanisms of selenium and/or selenoproteins on a shift towards anti-cancer. Int. Immunopharmacol. 96,. <https://doi.org/10.1016/j.intimp.2021.107790> 107790.
- Xiang, B., Yu, X., Li, B., Xiong, Y., Long, M., He, Q., 2019. Characterization, antioxidant, and anticancer activities of a neutral polysaccharide from *Duchesnea indica* (Andr.) Focke. J. Food Biochem. 43 (7), e12899.
- Zhan, T., Bai, Q., Zhao, Z., 2021. Antiproliferative effects of levan polysaccharide against colorectal cancer cells mediated through oxidative stress-stimulated HOTAIR/Akt signaling pathway: *In vitro*. Arab. J. Chem. 14, (12). <https://doi.org/10.1016/j.arabjc.2021.103389> 103389.
- Zhang, S., He, F., Chen, X., Ding, K., 2019. Isolation and structural characterization of a pectin from *Lycium ruthenicum* Murr and its anti-pancreatic ductal adenocarcinoma cell activity. Carbohydr. Polym. 223,. <https://doi.org/10.1016/j.carbpol.2019.115104> 115104.
- Zhang, S., An, L., Li, Z., Wang, H., Shi, L., Zhang, J., Li, Y., Jin, D. Q., Tuerhong, M., Ohizumi, Y., Shuai, L., Xu, J., Guo, Y., 2020a. An active heteropolysaccharide from the rinds of *Garcinia mangostana* Linn.: Structural characterization and immunomodulation activity evaluation. Carbohydr. Polym. 235,. <https://doi.org/10.1016/j.carbpol.2020.115929> 115929.
- Zhang, S., Li, Z., Wang, X., An, L., Bao, J., Zhang, J., Cui, J., Li, Y., Jin, D.Q., Tuerhong, M., Abudukeremu, M., Ohizumi, Y., Xu, J., Guo, Y., 2020b. Isolation, structural elucidation, and immunoregulation properties of an arabinofuranan from the rinds of *Garcinia mangostana*. Carbohydr. Polym. 246,. [https://doi.org/10.1016/j-carbpol.2020.116567](https://doi.org/10.1016/j.carbpol.2020.116567) 116567.
- Zheng, L., Ma, Y., Zhang, Y., Meng, Q., Yang, J., Gong, W., Liu, Q., Cai, L., Hao, L., Wang, B., Yang, Y., 2020. Distribution of Zinc in Mycelial Cells and Antioxidant and Anti-Inflammatory Activities of Mycelia Zinc Polysaccharides from *Thelephora ganbajum* TG-01. Oxid. Med. Cell. Longev. 2020, 2308017. <https://doi.org/10.1155/2020/2308017>.
- Zhong, H., Xiao, M., Zarkovic, K., Zhu, M., Sa, R., Lu, J., Tao, Y., Chen, Q., Xia, L., Cheng, S., Waeg, G., Zarkovic, N., Yin, H., 2017. Mitochondrial control of apoptosis through modulation of cardiolipin oxidation in hepatocellular carcinoma: A novel link between oxidative stress and cancer. Free Radic. Biol. Med. 102, 67–76. <https://doi.org/10.1016/j.freeradbiomed.2016.10.494>.
- Zhou, J., Zhang, D., Lv, X., Liu, X., Xu, W., Chen, L., Cai, J., Din, Z., Cheng, S., 2022. Green Synthesis of Robust Selenium Nanoparticles via Polysaccharide-Polyphenol Interaction: Design Principles and Structure-Bioactivity Relationship. ACS Sustain. Chem. Eng. 10 (6), 2052–2062. <https://doi.org/10.1021/acssuschemeng.1c06048>.
- Zhu, Z.Y., Liu, F., Gao, H., Sun, H., Meng, M., Zhang, Y.M., 2016. Synthesis, characterization and antioxidant activity of selenium polysaccharide from *Cordyceps militaris*. Int. J. Biol. Macromol. 93 (Pt A), 1090–1099. <https://doi.org/10.1016/j.ijbiomac.2016.09.076>.